Journal of Energy Chemistry 45 (2020) 25–30

Contents lists available at ScienceDirect

Journal of Energy Chemistry

journal homepage: www.elsevier.com/locate/jechem

http://www.journals.elsevier.com/journal-of-energy-chemistry/

Methylcyclopentenyl cation mediated reaction route in methanol-to-olefins reaction over H-RUB-50 with small cavity

Wenna Zhang[a,b], Shutao Xu[a], Yuchun Zhi[a], Yingxu Wei[a,*], Zhongmin Liu[a,*]

[a] National Engineering Laboratory for Methanol to Olefins, State Energy Low Carbon Catalysis and Engineering R&D Center, Dalian National Laboratory for Clean Energy, iChEM (Collaborative Innovation Center of Chemistry for Energy Materials), Dalian Institute of Chemical Physics, Chinese Academy of Sciences, Dalian 116023, Liaoning, China

[b] University of Chinese Academy of Sciences, Beijing 100049, China

ARTICLE INFO

Article history:
Received 22 August 2019
Revised 11 September 2019
Accepted 23 September 2019
Available online 3 October 2019

Keywords:
Methanol to olefins
H-RUB-50
Methylcyclopentenyl cation
Cyclopentadienes-based cycle

ABSTRACT

Methylcyclopentenyl cations (MCP^+) have been regarded as active intermediates during methanol conversion, however, their function mode in the reaction are still uncertain. In our recent report, trimethylcyclopentenyl cation ($triMCP^+$) and its deprotonated counterpart (trimethylcyclopentadiene, triMCP) were directly captured on H-RUB-50 catalyst with small cavity by the aid of in situ ^{13}C MAS NMR spectroscopy, and their higher catalytic reactivity were clarified by $^{12}C/^{13}C$-CH_3OH isotopic switch experiment. In this contribution, an alternative route—cyclopentadienes-based cycle was applied on methanol conversion catalyzed on the H-RUB-50, in which ethene was produced with the participation of $triMCP^+$ as critical intermediate. Then the cyclopentadienes-based cycle was predicted to be energetically favorable for ethene formation by density functional theory (DFT) calculations. The energetic comparison of paring mechanism in the aromatics-based cycle and cyclopentadienes-based cycle with the involvements of trimethylcyclopentadienyl ($triMCP_{di}^+$) and $triMCP^+$ as the corresponding active intermediates suggests that cyclopentadienes-based cycle is a feasible route for ethene formation. Furthermore, this work highlights the importance of the steric constraint and the host-guest interaction induced by the zeolite with cavity structure in the formation of intermediates and reaction pathway.

1. Introduction

With the increasing market demand of light olefins and the depletion of oil resources, methanol-to-olefins (MTO) conversion, as a non-petrochemical route for the production of light olefins from coal and natural gas etc., has attracted great interest over the past 40 years [1–6]. In 2010, a major commercialization breakthrough of MTO process developed by Dalian Institute of Chemical Physics has been achieved [4,5]. Meanwhile, great efforts have been devoted to a better understanding of MTO reaction mechanism, which is important for both of fundamental research and commercial application.

In light of the complex nature of methanol conversion catalyzed by the zeolites and zeotype catalysts, a thorough understanding of MTO mechanism remains a challenge. At present, indirect reaction mechanism is widely accepted in the MTO reaction [5–9]. It involves active intermediates (e.g., alkenes [10–12], cyclopentadienes [13–20] and aromatics [14,21–24]) acting as co-catalysts. These intermediates can react with methanol to realize the growth of C–C bond, and then split off olefins. However, the relative reactivity of the active intermediates, their origins and their reaction pathway are still not well interpreted.

Organic intermediate species were captured and identified as active intermediates by the aid of experimental studies and theoretical calculations. Polymethylbenzenium [14,21–24], polymethylcyclopentenyl cations [13–20] and their corresponding neutral species, along with alkene species, were confirmed as important intermediates or co-catalysts for the light olefins formation. Based on these active organic species, aromatics-based cycle (side-chain methylation [25] and paring mechanism [26]) and alkenes-based cycle [10,11,27] were proposed to elucidate the generation of olefins. The reaction network of the indirect mechanism was established based on these proposed catalytic pathways. Other new reaction pathway with feasible energy and the potential active intermediates require more investigations.

In our previous studies, we directly observed MCP^+ on the 8-membered ring (8-MR) and cavity-type zeolite, such as pentamethylcyclopentenyl cation ($pentaMCP^+$) over DNL-6 [21],

* Corresponding authors.
E-mail addresses: weiyx@dicp.ac.cn (Y. Wei), liuzm@dicp.ac.cn (Z. Liu).

https://doi.org/10.1016/j.jechem.2019.09.022

SSZ-13 [14], and SAPO-34 [16], triMCP$^+$ over SAPO-35 [16] and H-RUB-50 [19]. With respect to the traditional aromatics-based cycle, methylcyclopentadienyl cation (MCP_{di}^+) acting as key intermediates in the paring mechanism [14,17,18,26] have been examined in detail. However, the catalytic cycle involving these methylcyclopentenyl cations (MCP$^+$, structurally differing from the MCP_{di}^+ in paring mechanism) as the direct intermediates to form light olefins have rarely been reported. It is worthy to note that higher reactivity of the methylcyclopentadienes (MCP) has been confirmed by $^{13}C/^{12}C$-isotopic methanol switch technique [19]. Thus, the role of MCP$^+$ and neutral MCP should be taken into account in methanol conversion.

In our recent study, we investigated the formation and reactivity of MCP$^+$ in detail, and proposed a novel cyclopentadienes-based cycle for methanol conversion over H-SAPO-34 [28]. In this newly proposed cycle, MCP$^+$ and MCP species can directly participate the catalytic cycle for light olefins formation over H-SAPO-34. For H-SAPO-34 (6.7 × 10 Å) with bulky-sized CHA cavity, pentaMCP$^+$ was identified as active species [28], while as for H-RUB-50 with small cavity (6.3 × 7.3 Å), triMCP$^+$ presents less methyl groups substitution [19,28]. Such variation in the number of methyl group substitution of the confined organic intermediates reflects the confinement effect of cavity structure, originating from the host-guest interaction of zeolite-catalyzed reaction system. Simultaneously, small-sized cavity structure with steric constraint may modulate the reaction pathway with the participation of the small-sized active intermediates. This encourages us to continuously establish and study all the potential reaction routes of MTO catalyzed on the zeolite with small-sized cavity.

In the present work, based on the report of the capture of the triMCP$^+$ with less methyl group substitution and higher reactivity of its neutral triMCP, a cyclopentadienes-based cycle working as an alternative catalytic cycle for methanol conversion was established. DFT theoretical calculations were performed to examine the feasibility of the cyclopentadienes-based cycle from energetic perspective. Two cyclic carbenium ions (MCP_{di}^+ and MCP$^+$) in their respective catalytic cycles (the paring cycle and cyclopentadienes-based cycle) were investigated in detail. A deep understanding of the cavity-controlled principle was provided based on the variation of the intermediate and reaction pathway imposed by host-guest interaction from the cavity structure.

2. Experimental section and theoretical calculation

2.1. Experimental section

The synthesis procedure and characterization of H-RUB-50 and the catalytic performances of methanol conversion at different temperatures have been reported in our previous study [19]. The determination of confined organics with GC–MS and ^{13}C solid-state MAS NMR is displayed in the Supporting Information.

2.2. Theoretical calculation

For theoretical calculations, a 52T cluster model ($Si_{51}AlO_{82}H_{45}$) represents the structure of H-RUB-50 zeolite as shown in Fig. 1, which was extracted from the crystallographic LEV structure. In the theoretical calculations for the extended zeolite model, the terminal Si–H was fixed at a bond length of 1.47 Å, oriented along the direction of the corresponding Si–O bond. The locations of acid sites were chosen at the 8-MR window, accessible for adsorbents and surrounded by maximum reaction space [29]. The substituted Al atom was placed at the T2 site of the crystallographic position during structural optimization.

The combined theoretical ONIOM method [30–32] was applied to predict the geometries of various adsorption structures and transition states (TS). During the structure optimization, ωB97XD hybrid density function with 6–31 G (d, p) basis sets and semi-empirical AM1 were employed for optimizing geometries of the high-level and low-level layer. The ωB97XD method is the hybrid meta DFT developed by Chai and Head-Gordon, where implicitly accounts for empirical dispersion and can describe long-range dispersion interactions well with respect to the traditional DFT methods [33]. To preserve the integrity of the zeolite structure during the structure optimizations, the 8-MR window, $(SiO)_3$–Si–OH–Al–$(SiO)_3$ active center and the adsorbed species in the high-level layer were relaxed while the rest of atoms were fixed in the low-level at their crystallographic locations. To obtain highly accurate energies, the single-point energies were calculated at the level of ωB97XD/6–31 G (d, p) on the basis of optimized structures. The frequency calculations were performed at the same level as geometry optimizations to check whether the saddle points exhibit the proper number of imaginary frequencies. Only a single imaginary frequency was observed for the transition state, and no imaginary frequency was observed for the adsorbed state. The intrinsic free energy barrier ($\Delta G^{\ddagger}$) at 300 °C for each elementary reaction in a completed reaction route was obtained from the ωB97XD/6–31 G (d, p) total electronic energies and the thermal correction from the ωB97XD/6–31 G (d, p): AM1 frequency calculations. All density functional theory (DFT) calculations were performed with the Gaussian 09 package [34].

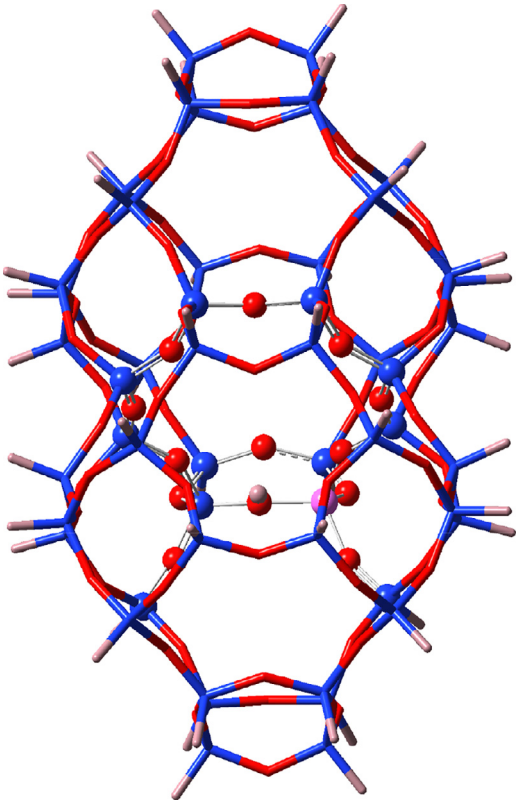

Fig. 1. Representations of H-RUB-50 framework structures by 52T cluster models. The 8-MR window and $(SiO)_3$–Si–OH–Al–$(SiO)_3$ active center in the extended cluster model represented as ball and stick view is treated as the high-layer atoms during the ONIOM calculations.

3. Results and discussion

3.1. Observation of the MCP$^+$ and reactivity confirmation of MCP

MCP$^+$ and their deprotonated forms (MCP) confined in zeolite or SAPOs catalysts have been identified using ^{13}C NMR,

Table 1. Carbenium ions observed in H-RUB-50 with solid-state NMR and the ^{13}C content (%) of their deprotonated counterparts obtained by $^{12}C/^{13}C$-methanol switch experiments.

Carbenium ions	Deprotonated counterparts	Relative ^{13}C content (%)
	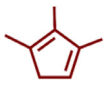	45.80
		34.70
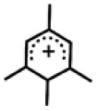	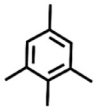	33.87

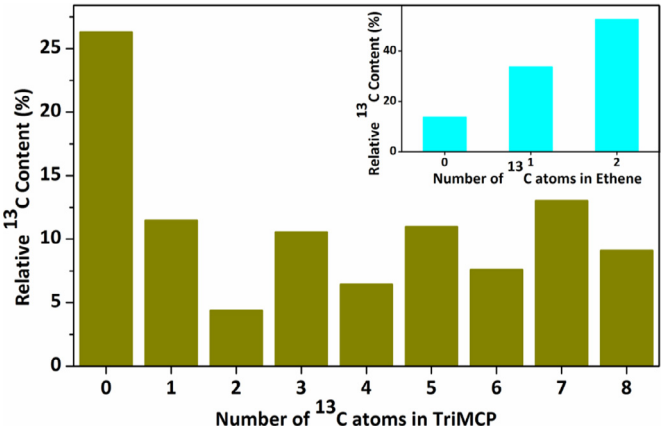

Fig. 2. Isotopic distribution of triMCP formed after the $^{12}C/^{13}C$-methanol switch experiments over H-RUB-50 at 350 °C after 25 min of ^{12}C-methanol reaction followed by 1 min of ^{13}C-methanol reaction. Inset: the isotopic distribution of ethene.

UV–vis spectroscopy and theoretical calculations [13–20,35]. Table 1 and Figs. S1 and S2 in supporting information summarized carbenium ions observed in H-RUB-50 with ^{13}C solid-state NMR and the relative ^{13}C content of their deprotonated counterparts obtained by $^{12}C/^{13}C$-methanol switch experiments [19]. Combined with the previous theoretical calculation, 1, 2, 5-triMCP$^+$, 1, 2, 3-trimethylbenzenium (triMB$^+$) and 1, 3, 4, 5-tetramethylbenzenium (tetraMB$^+$) cations were ascertained to be the essential reactive intermediates [19]. And triMCP and tri/tetramethylbenzenes (tri/tetraMB) exhibit higher ^{13}C content than other components (penta/hexaMB, 20%), suggesting that these intermediates may act as co-catalytic active centers for methanol conversion. Especially, triMCP exhibits very high ^{13}C content of 45.80%. The capture of triMCP$^+$ and higher reactivity of triMCP implied their important role as critical intermediates in the MTO reaction.

Fig. 2 shows the isotopic distribution of triMCP and ethene formed after the $^{12}C/^{13}C$-methanol switch experiments over H-RUB-50 at 350 °C after 25 min of ^{12}C-methanol reaction followed by 1 min of ^{13}C-methanol reaction. Ethene was found to contain both ^{12}C and ^{13}C atoms suggesting that ethene is formed via the interaction of ^{13}C-methanol and the confined ^{12}C-carbenium ions. In addition, the random isotopic distribution of triMCP confirms the participation of triMCP$^+$/triMCP as the active species in the methanol conversion.

Notably, MCP$^+$ have been captured widely on various zeolites and molecular sieve catalysts with different topological structure. As listed in Table 2, 1, 3-dimethylcyclopentenyl (diMCP$^+$), 1, 3, 4-triMCP$^+$ and ethylcyclopentenyl (ECP$^+$) cations on H-ZSM-5 [17,18] tri/tetraMCP$^+$ cation on SAPO-35 [16] and heptamethylcyclopentenyl (heptaMCP$^+$), pentaMCP$^+$ on H-SAPO-34 [16,28], H-Beta [36],

Table 2. Methylcyclopentenyl (MCP$^+$) cations formed on zeolite or SAPOs catalysts (e.g., H-ZSM-5 [17,18], SAPO-34 [16], SSZ-13 [14], SAPO-35 [16], H-Beta [35], DNL-6 [21], H-RUB-50) in MTO reaction.

Catalysts	MCP$^+$	Cations
H-ZSM-5	diMCP$^+$triMCP$^+$ECP$^+$	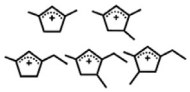
SAPO-34	petaMCP$^+$heptaMCP$^+$	
SAPO-35	triMCP$^+$	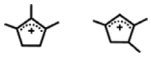
H-BetaSSZ-13DNL-6	petraMCP$^+$	
H-RUB-50	triMCP$^+$	

DNL-6 [21] and SSZ-13[14] were unambiguously identified as critical intermediates for catalyzing mthanol conversion by employing the combined techniques of ^{13}C MAS NMR, GC–MS, and theoretical calculations. The structures of these MCP$^+$ are closely related to the chemical environment of molecular sieve. For the critical intermediates on the H-RUB-50, the small-sized intermediate (triMCP$^+$) with less methyl group was observed, which is ascribed to the steric constraint of small cavity structure. In MTO reaction, the variation in topological structure of zeolites would vary the chemical structure of these cyclic organic species formed in the catalysts and their detailed reaction route for converting methanol. This suggests indirect pathway of MTO reaction is associated with the host-guest interaction of the confined organic intermediates and inorganic zeolite framework.

As for H-RUB-50, based on the experimental observation and identification of triMCP (triMCP$^+$), triMB (triMB$^+$) and tetraMB (tetraMB$^+$) intermediates, the traditional aromatics-based cycle (consisting of side-chain methylation and paring mechanisms) are examined via theoretical evaluation in our previous work [19]. As above discussed, triMCP$^+$/triMCP was identified as another kind of critical intermediates with the higher reactivity. So, next, an alternative cyclopentadienes-based cycle with the involvement of triMCP$^+$ as independent active intermediate will be proposed for ethene formation. Theoretical calculation was carried out to verify the feasibility of this catalytic cycle.

3.2. Theoretical calculation of ethene formation via cyclopentadienes-based cycle with the participation of triMCP$^+$

The reaction route of cyclopentadienes-based cycle is established based on the participation of the (triMCP$^+$) (the protonated form of triMCP) as direct intermediates, which starts from deprotonation step (**D1**) of TriMCP$^+$ as shown in Scheme 1. Then, methanol molecular attacks the formed dimethylmethyleneycyclopentadiene with an exocyclic double bond to get 2, 3-dimethyl-1-ethylcyclopentenyl cation via an exocyclic methylation (**M1**). This cation is the crucial precursor for ethene formation with ethyl side-chain. Subsequently, 4, 5-dimethyl-2-ethylcyclopentenyl cation is obtained through hydride/ethyl-transfer step, followed by the ethene elimination (**E1**) to generate ethene. Next, the simultaneously formed dimethylcyclopentadiene gets methylated (**M2**) to form trimethylcyclopentenyl cation over the restored Brϕnsted acid sites. Eventually, triMCP$^+$ is recovered via hydride/methyl-transfer step.

The detailed calculated free energy barriers and the Gibbs free energy profile of all the elementary steps of cyclopentadienes-based cycle at 300 °C is shown in Fig. 3. The

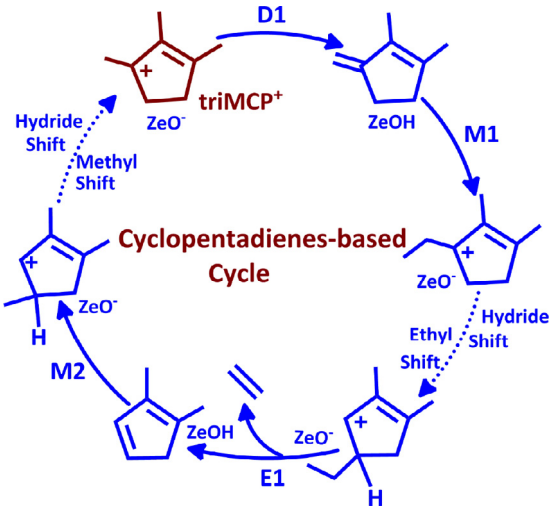

Scheme 1. The cyclopentadienes-based catalytic cycle with participation of triMCP$^+$ for the formation of ethene for methanol reaction over H-RUB-50.

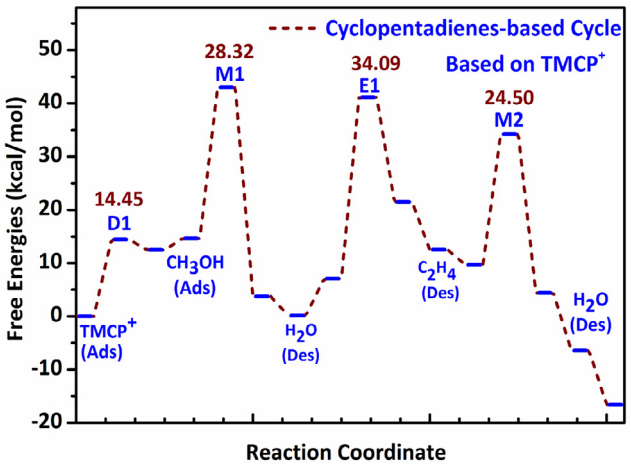

Fig. 3. Gibbs free energy profile for methanol conversion to ethene over H-RUB-50 following the cyclopentadienes-based cycle with participation of triMCP$^+$ at 300 °C.

cyclopentadienes-based cycle can be realized via simple methylation and elimination to fulfill the propagation of C–C bond and the olefins formation. In this catalytic cycle, two methylation steps of the exocyclic double bond (**M1**) and the ring (**M2**) need to overcome the energy barrier of 28.32 and 24.50 kcal/mol, respectively. The elimination of ethene (**E1**) is predicted with the free energy barrier of 34.09 kcal/mol. All the elementary steps need the relatively lower energy barrier of 14.45–34.09 kcal/mol. The overall energetic span of the whole catalytic cycle is around 42.95 kcal/mol. Compared to the traditional aromatics-based cycle and alkenes-based cycle, the cyclopentadienes-based cycle is an energetically feasible route for olefins formation [14,19].

Lower energy barriers of all the elementary steps and the energetic span on the whole catalytic cycle suggest that the cyclopentadienes-based cycle with the involvement of triMCP$^+$ can operate as an alternative route for ethene formation. Therefore, ethene can be formed via multiple routes of methanol conversion on H-RUB-50, i.e., cyclopentadienes-based cycle, aromatics-based cycle (side-chain methylation and paring route).

3.3. Cyclopentadienes-based cycle versus paring cycle with the involvements of MCP$^+$ and MCP$_{di}^+$ cations

Two cyclic carbenium ions (MCP$^+$ and MCP$_{di}^+$), as shown in Scheme 2, have been reported in the methanol conversion

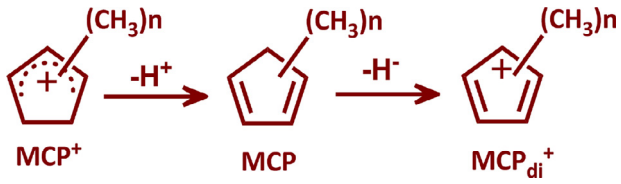

Scheme 2. Two cyclic carbenium ions and the conversion of MCP$^+$, MCP and MCP$_{di}^+$ in the methanol conversion (methylcyclopentenyl cation: MCP$^+$; methylcyclopentadiene: MCP; methylcyclopentadienyl cation: MCP$_{di}^+$).

Table 3. Calculated free energy barriers ($\Delta G^{\ddagger}$) of the rate-determining step and the energetic span at 300 °C for ethene formation via cyclopentadienes-based cycle and paring cycle [19] in methanol conversion over H-RUB-50 zeolite.

	Cyclopentadienes-based cycle	Paring cycle
Rate-determining step(kcal/mol)	34.09	45.80
Energetic span(kcal/mol)	42.95	77.21

catalyzed by zeolite or SAPOs. The cyclopentadienyl cations (MCP$_{di}^+$), as the isomerized species of benzenium cations, are generally involved in the paring mechanism of aromatics-based cycle, which is proposed in 1961 by Sullivan et al. [37] The paring mechanism involves the ring contraction/expansion reactions of MCP$_{di}^+$ and aromatics species to produce cyclic organics with alkyl side chain as the olefins precursors, which then split off olefins. Another cation of MCP$^+$ appeared in the experimental observation can participate as a direct intermediate in the cyclopentadienes-based cycle to generate olefins.

The role and reactivity of these two cyclic carbenium ions (MCP$^+$, MCP$_{di}^+$) in the paring cycle [19] and cyclopentadienes-based cycle were investigated in detail. Comparison of the calculated free energy barriers ($\Delta G^{\ddagger}$) of the elementary reactions for ethene formation via paring cycle and cyclopentadienes-based cycle at 300 °C is depicted in Scheme 3. For the sequence of the two cycles, paring cycle including more complex reaction steps undergoes successive contraction/expansion, methylation, elimination and series of transfer reactions. In the cyclopentadienes-based cycle, the species with exocyclic double bond can methylate with methanol to form the olefins precursors that can directly split off olefins. In the paring route [19], methylation of trimethylbenzene (**M1**) and the formation of dimethylbenezene (**P4b**) need to overcome free energy barriers of 37.01 and 36.38 kcal/mol, which are higher than the barriers of methylation steps (**M1**, 28.32 kcal/mol; **M2**, 24.50 kcal/mol) in the cyclopentadienes-based cycle. This conforms to the fact that the small cavity structure tends to form the small-sized intermediates due to the steric constraint of small cavity structure in H-RUB-50. Specifically, the rate-determining step in the paring route (**E1**) has higher energy barrier (45.80 kcal/mol). Rather, in the cyclopentadienes-based cycle, the reaction proceeds with lower free energy barrier (14.45–34.09 kcal/mol).

It should be noted that the rate-determining step in cyclopentadienes-based and paring cycle is elimination reaction, different from that in side-chain methylation route with methylation reaction as rate-determining step [19]. This illustrates that H-RUB-50 with small LEV cavity allows cyclopentadienes-based and paring cycles with the involvements of triMCP$_{di}^+$ and triMCP$^+$ as active centers, while the formation of bulky-sized precursors in side-chain methylation route exhibits steric constraint of small cavity in H-RUB-50. In the cyclopentadienes-based and paring cycle, small-size precursors formed from methylation of five-member ring species, are not limited by the small cavity. Therefore, the elimination reaction in the cyclopentadienes-based and paring cycle turns into the rate-determining step.

Table 3 provides the detailed free energy barriers ($\Delta G^{\ddagger}$) of the rate-determining step and energetic span at 300 °C for ethene

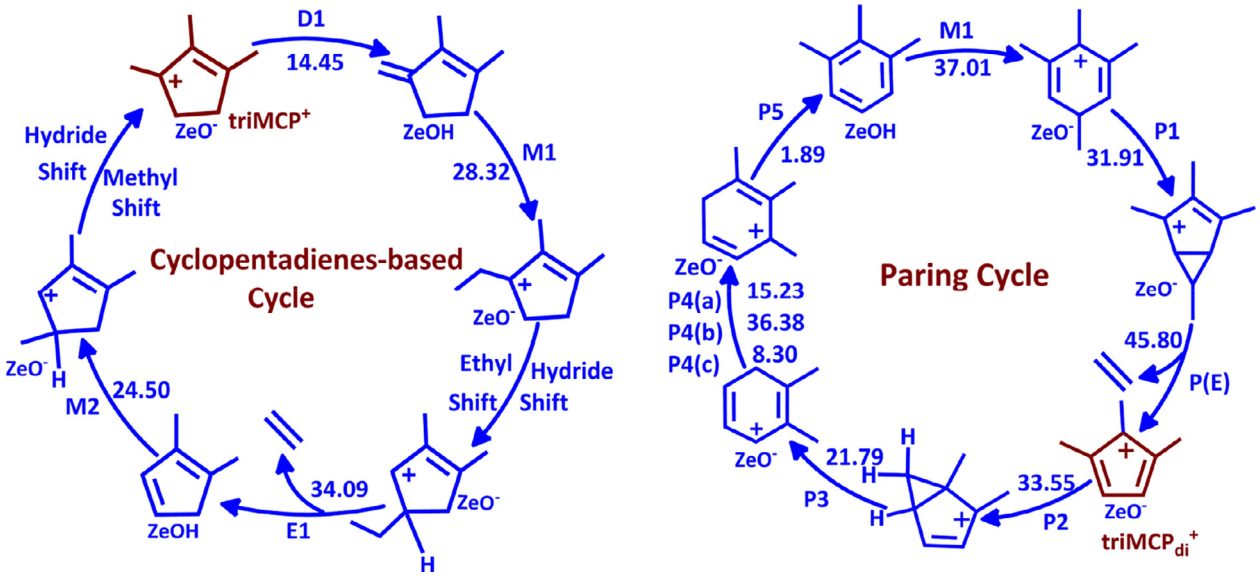

Scheme 3. Ethene formation via cyclopentadienes-based cycle and paring cycle [19]) in methanol conversion over H-RUB-50. Calculated free energy barriers at 300 °C are given in kcal/mol.

formation via cyclopentadienes-based cycle and paring cycle. For the elimination of ethene, the energy of the rate-determining step in the paring cycle (45.80 kcal/mol) is higher by 11 kcal/mol than that in cyclopentadienes-based cycle (34.09 kcal/mol). The energy span of the cyclopentadienes-based cycle (42.95 kcal/mol) is much less than that of the paring cycle (77.21 kcal/mol) [19] by about 35 kcal/mol in H-RUB-50. And the value of the energy span in the cyclopentadienes-based cycle is comparable to that in the aromatics-based cycle (41.62 kcal/mol) [19], indicating the energetic feasibility of the cyclopentedienes-based cycle. The lower energy span in the side-chain methylation reveals that it is more energetically favorable for the formation of ethene. Importantly, similar value between cyclopentadienes-based cycle and aromatics-based cycle (side-chain methylation) suggests that two catalytic cycle work together for ethene formation of MTO reaction over H-RUB-50. TriMCP$^+$ and its deprotonated counterpart (triMCP) can behave as the co-catalytic species and mediate the reaction pathway in H-RUB-50.

4. Conclusions

In summary, triMCP$^+$ and its deprotonated counterpart (triMCP) with less methyl group substitution were confirmed as critical intermediates on H-RUB-50. Based on the higher reactivity of these small-sized intermediates, a novel cyclopentadienes-based cycle with the involvement of triMCP$^+$ as a direct intermediate was established for ethene formation. The DFT calculation verifies that this cyclopentadienes-based cycle is energetically feasible route for ethene formation in H-RUB-50. The comparison of paring cycle and cyclopentadienes-based cycle with the involvements of triMCP$_{di}^+$ and triMCP$^+$ cations as active intermediates further confirm the feasibility of the cyclopentadienes-based cycle. Furthermore, the variation of the intermediate and reaction pathway induced by the special host-guest interaction of methanol conversion catalyzed on the cavity structure offers the evidence of the cavity-controlled principle of methanol conversion.

Acknowledgments

The authors thank the financial support from the National Natural Science Foundation of China (Nos. 91745109, 21703239 and 21972142), the Key Research Program of Frontier Sciences, CAS, Grant No. QYZDY-SSW-JSC024, the Youth Innovation Promotion Association of the Chinese Academy of Sciences (No. 2014165), the International Partnership Program of Chinese Academy of Sciences, Grant No. 121421KYSB20180007 and Liaoning Revitalization Talents Program (XLYC1807227).

Supplementary materials

Supplementary material associated with this article can be found, in the online version, at doi:10.1016/j.jechem.2019.09.022.

References

[1] M. Stocker, Microporous Mesoporous Mater. 29 (1999) 3–48.
[2] U. Olsbye, S. Svelle, M. Bjorgen, P. Beato, T.V. Janssens, F. Joensen, S. Bordiga, K.P. Lillerud, Angew. Chem. Int. Ed. 51 (2012) 5810–5831.
[3] S. Ilias, A. Bhan, ACS Catal. 3 (2013) 18–31.
[4] P. Tian, Y. Wei, M. Ye, Z. Liu, ACS Catal. 5 (2015) 1922–1938.
[5] S. Xu, Y. Zhi, J. Han, W. Zhang, X. Wu, T. Sun, Y. Wei, Z. Liu, Adv. Catal. 61 (2017) 37–122.
[6] I. Yarulina, A.D. Chowdhury, F. Meirer, B.M. Weckhuysen, J. Gascon, Nat. Catal. 1 (2018) 398–411.
[7] I.M. Dahl, S. Kolboe, Catal. Lett. 20 (1993) 329–336.
[8] I.M. Dahl, S. Kolboe, J. Catal. 149 (1994) 458–464.
[9] I.M. Dahl, S. Kolboe, J. Catal. 161 (1996) 304–309.
[10] M. Bjorgen, S. Svelle, F. Joensen, J. Nerlov, S. Kolboe, F. Bonino, L. Palumbo, S. Bordiga, U. Olsbye, J. Catal. 249 (2007) 195–207.
[11] C.-.M. Wang, Y.-.D. Wang, Z.-.K. Xie, J. Catal. 301 (2013) 8–19.
[12] W. Dai, M. Dyballa, G. Wu, L. Li, N. Guan, M. Hunger, J. Phys. Chem. C 119 (2015) 2637–2645.
[13] J.F. Haw, J.B. Nicholas, W.G. Song, F. Deng, Z.K. Wang, T. Xu, C.S. Heneghan, J. Am. Chem. Soc. 122 (2000) 4763–4775.
[14] S. Xu, A. Zheng, Y. Wei, J. Chen, J. Li, Y. Chu, M. Zhang, Q. Wang, Y. Zhou, J. Wang, F. Deng, Z. Liu, Angew. Chem. Int. Ed. 52 (2013) 11564–11568.
[15] M.J. Wulfers, F.C. Jentoft, ACS Catal. 4 (2014) 3521–3532.
[16] J. Li, Y. Wei, J. Chen, S. Xu, P. Tian, X. Yang, B. Li, J. Wang, Z. Liu, ACS Catal. 5 (2015) 661–665.
[17] C. Wang, Y. Chu, A. Zheng, J. Xu, Q. Wang, P. Gao, G. Qi, Y. Gong, F. Deng, Chem. Eur. J. 20 (2014) 12432–12443.
[18] C. Wang, X. Yi, J. Xu, G. Qi, P. Gao, W. Wang, Y. Chu, Q. Wang, N. Feng, X. Liu, A. Zheng, F. Deng, Chem. Eur. J. 21 (2015) 12061–12068.
[19] W. Zhang, J. Chen, S. Xu, Y. Chu, Y. Wei, Y. Zhi, J. Huang, A. Zheng, X. Wu, X. Meng, F. Xiao, F. Deng, Z. Liu, ACS. Catal. 8 (2018) 10950–10963.
[20] W.G. Song, J.B. Nicholas, J.F. Haw, J. Phys. Chem. B 105 (2001) 4317–4323.
[21] J. Li, Y. Wei, J. Chen, P. Tian, X. Su, S. Xu, Y. Qi, Q. Wang, Y. Zhou, Y. He, Z. Liu, J. Am. Chem. Soc. 134 (2012) 836–839.
[22] T. Xu, D.H. Barich, P.W. Goguen, W.G. Song, Z.K. Wang, J.B. Nicholas, J.F. Haw, J. Am. Chem. Soc. 120 (1998) 4025–4026.

[23] W. Dai, M. Scheibe, N. Guan, L. Lan, M. Hunger, ChemCatChem 3 (2011) 1130–1133.
[24] W.G. Song, H. Fu, J.F. Haw, J. Am. Chem. Soc. 123 (2001) 4749–4754.
[25] B. Arstad, J.B. Nicholas, J.F. Haw, J. Am. Chem. Soc. 126 (2004) 2991–3001.
[26] D.M. McCann, D. Lesthaeghe, P.W. Kletnieks, D.R. Guenther, M.J. Hayman, V. Van Speybroeck, M. Waroquier, J.F. Haw, Angew. Chem. Int. Ed. 120 (2008) 5257–5260.
[27] D. Lesthaeghe, J. Van der Mynsbrugge, M. Vandichel, M. Waroquier, V. Van Speybroeck, ChemCatChem 3 (2011) 208–212.
[28] W. Zhang, Y. Zhi, J. Huang, X. Wu, S. Zeng, S. Xu, A. Zheng, Y. Wei, Z. Liu, ACS Catal. 9 (2019) 7373–7379.
[29] P.J. O'Malley, J. Dwyer, Zeolites 8 (1988) 317–321.
[30] Y. Chu, B. Han, A. Zheng, F. Deng, J. Phys. Chem. C 116 (2012) 12687–12695.
[31] D. Lesthaeghe, B. De Sterck, V. Van Speybroeck, G.B. Marin, M. Waroquier, Angew. Chem. Int. Ed. 46 (2007) 1311–1314.
[32] D.K. Papayannis, K.D. Papavasileiou, V.S. Melissas, Microporous Mesoporous Mater. 226 (2016) 1–9.
[33] J.D. Chai, M. Head-Gordon, Phys. Chem. Chem. Phys. 10 (2008) 6615–6620.
[34] M.J. Frisch, G. W.Trucks, H.B. Schlegel, G.E. Scuseria, M.A. Robb, J.R. Cheeseman, G. Scalmani, V. Barone, B. Mennucci, G.A. Petersson, H. Nakatsuji, M. Caricato, X. Li, H.P. Hratchian, A.F. Izmaylov, J. Bloino, G. Zheng, J.L. Sonnenberg, M. Hada, M. Ehara, K. Toyota, R. Fukuda, J. Hasegawa, M. Ishida, T. Nakajima, Y. Honda, O. Kitao, H. Naka, T. Vreven, J.A. Montgomery, J. E.Peralta, F. Ogliaro, M. Bearpark, J.J. Heyd, E. Brothers, K.N. Kudin, V.N. Staroverov, R. Kobayashi, J. Normand, K. Raghavachari, A. Rendell, J.C. Burant, S.S. Iyengar, J. Tomasi, M. Cossi, N. Rega, J.M. Millam, M. Klene, J.E. Knox, J.B. Cross, V. Bakken, C. Adamo, J. Jaramillo, R. Gomperts, R.E. Stratmann, O. Yazyev, A.J. Austin, R. Cammi, C. Pomelli, J.W. Ochterski, R.L. Martin, K. Morokuma, V.G. Zakrzewski, G.A. Voth, P. Salvador, J.J. Dannenberg, S. Dapprich, A.D. Daniels, O. Farkas, J.B. Foresman, J.V. Ortiz, J. Cioslowski, D.J. Fox, Gaussian 09, Revision B.01, Gaussian, Inc., Wallingford, CT, 2010.
[35] C. Wang, X. Sun, J. Xu, G. Qi, W. Wang, X. Zhao, W. Li, Q. Wang, F. Deng, J. Catal. 354 (2017) 138–151.
[36] M. Zhang, S. Xu, J. Li, Y. Wei, Y. Gong, Y. Chu, A. Zheng, J. Wang, W. Zhang, X. Wu, F. Deng, Z. Liu, J. Catal. 335 (2016) 47–57.
[37] R.F. Sullivan, R.P. Sieg, G.E. Langlois, C.J. Egan, J. Am. Chem. Soc. 83 (1961) 1156–1160.